JOURNAL OF MATERIALS SCIENCE: MATERIALS IN ELECTRONICS 8 (1997) 115–123

Effects of spinel phase formation in the calcination process on the characteristics of ZnO–glass varistors

YIH-SHING LEE, TSEUNG-YUEN TSENG
Department of Electronics Engineering and Institute of Electronics, National Chiao-Tung University, Hsinchu, Taiwan

Ceramic varistors based on ZnO with lead zinc borosilicate glass were prepared in order to study the effects of various calcination processes on the formation of spinel phase during the sintering process, including the effects of different temperatures and soaking times. A ZnO–glass sample was prepared using powder calcined at 600 °C for 10 h then sintered at 1250 °C for 1 h; this sample possessed the highest non-linear coefficient, breakdown voltage and non-linear resistance as well as the lowest leakage current. The optimum amount of $Zn_7Sb_2O_{12}$ spinel phase, formed in the calcination process, that can inhibit ZnO grain growth in the subsequent sintering plays an important role in the grain size distribution and stability of ZnO–glass ceramic varistors. Uniform distribution of the grain size obtained from suitable calcination processes was an important microstructural parameter in achieving a good device stability of ZnO–glass varistors. The dynamic resistance and the non-linear resistance of the ZnO–glass varistor, correlated with the average grain size, were proposed to describe insulating characteristics of the varistor samples. Increases in these two parameters, created by decreasing the grain size, enhances the sample clamping voltage during the surge impact and the sample breakdown voltage.

1. Introduction

Zinc oxide varistors [1–3] with additives of Bi_2O_3, Sb_2O_3, Co_2O_3, MnO_2 and Cr_2O_3 are non-linear resistors whose primary function is to sense and limit transient voltage surges and to do so repeatedly without being destroyed [4]. Inada [5, 6] reported that ZnO ceramic varistors consist of ZnO phase dissolving Co and Mn; spinel phase of $Zn_7Sb_2O_{12}$ containing Co, Mn and Cr; and Bi-rich phases.

Wong [7] has reported on the intergranular pyrochlore phase, $Bi_2(Zn_{4/3}Sb_{2/3})O_6$, which is stable at low temperatures in the ZnO–Bi_2O_3 ceramics. The spinel phase, transformed from the pyrochlore phase at elevated temperatures would act as a grain modulator for ZnO grains by anchoring the boundaries during sintering. Inada [5] has reported that spinel phase formed at temperatures above 700 °C gradually increases with an increase of sintering temperature and remarkably increases with the disappearance of the pyrochlore-type cubic phase. Mah *et al.* [8] have indicated that, in the subsequent sintering process, the primary spinel phase and the spinel phase transformed from the pyrochlore phase can raise the non-linear resistance by inhibiting ZnO grain growth. Also, the homogeneity of the grain size distribution plays an important role in determining the electrical properties of ZnO varistors [9–11]. Bai *et al.* [10] have reported that varistor samples made using small, uniform and spherical ZnO powders gave uniform microstructure and better non-ohmic properties. As reported in a previous paper [12], ZnO–glass varistors are excellent non-ohmic devices which are composed of three phases; ZnO grain, spinel phase of $Zn_7Sb_2O_{12}$ and crystallized intergranular glass phase. In the sintering process, the intergranular layer may be a grain growth inhibitor [13, 14], especially when it has a higher SiO_2 content. The phases of the ZnO–glass system are quite similar to those of the ZnO–Bi_2O_3 system [15–17], but intergranular glass phase replaces the Bi_2O_3 phase and there is no pyrochlore phase, $Bi_2(Zn_{4/3}Sb_{2/3})O_6$.

The purpose of this paper is to study how the formation of primary spinel phase, during the calcination process, affects the characteristics of ZnO–glass varistors and device stability. Quantitative analysis using X-ray diffraction (XRD) together with statistical distribution of the grain size from scanning electron microscopy (SEM) observation are applied to examine the effect of the spinel phase on inhibiting ZnO grain growth in the subsequent sintering and its effect on device stability. By means of a surge-withstanding test using a constant current source surge network, the dynamic resistance of ZnO–glass samples, $R_{ZnO-glass}$, is also proposed to describe the insulating characteristics of the varistor samples.

0957–4522

2. Experimental procedure

2.1. Sample preparation

ZnO–glass ceramic varistors were prepared by using a conventional technique. The glass powder, composition 10.93 wt% SiO_2, 19.25 wt% B_2O_3, 64.25 wt% PbO, and 5.29 wt% ZnO, used for preparing the ZnO–glass samples was analysed using inductively coupled plasma atomic emission spectroscopy (ICP-AES, Perkin-Elmer, Sciex Elan 5000). After mixing the raw materials in the proportions 95 mol% ZnO, 1 mol% CoO, 1 mol% MnO, 1 mol% Cr_2O_3, 2 mol% Sb_2O_3 and 10 wt% glass powder, they were wet-milled and dried at 250 °C; the powders were calcined at 600–900 °C for 2 h and 10 h. The calcined powders were ground, sifted through a 325-mesh screen and formed at a pressure of 2000 psi (14 MPa) into discs 10 mm in diameter and 1.5 mm in thickness. All sinterings were performed at 1250 °C in air for 1 h and cooled at a rate of 5 °C min^{-1} to 1000 °C, then furnace-cooled.

2.2. Electrical measurements

Conductive Ag paste coatings of 6.2 mm in diameter were applied at the centre of both sides of the sintered samples (8.2 mm in diameter and 1.25 mm in thickness) and heat treated at 110 °C for 10 min. The I–V characteristics of the varistor samples were measured using an a.c. power supply at a given operating voltage, and I–V data were read from a curve tracer (Tektronix, model 370A). The frequency of the a.c. power supply was 60 Hz. The I–V characteristics of ZnO varistors are expressed by the empirical equation [1, 8]

$$I = (V/C)^{\alpha} \quad (1)$$

where the non-linear resistance, C, is defined by a voltage drop per unit length (V mm^{-1}) when 1 mA cm^{-2} of current flows through the body; the non-linear coefficient, α, is determined by the equation [12]

$$\alpha = 1/\log(V_{10\ mA}/V_{1\ mA}) \quad (2)$$

using two measured voltage values, $V_{10\ mA}$ and $V_{1\ mA}$ at 10 and 1 mA currents, respectively. V_{br} represents the breakdown voltage of the varistor, which is the voltage value when the current value is 1 mA; I_{leak} represents the leakage current of the varistor at room temperature when the voltage value is 0.8 V_{br}.

The surge-withstanding capabilities and pulse tests were measured with a surge generator (Key-Tek, 801-plus) with a voltage–current combined surge wave. The $\Delta V_{br}/V_{br}$ values of the stable varistors lie within $\pm 10\%$ even at 26.1 A peak surge current and 1252 V applied voltage. The surge network is described in the next section.

2.3. Microstructural examination

The fractured surfaces of the sintered samples were lapped, ground and polished with 1 μm Al_2O_3 powder to a mirror-like surface. The surface microstructure was then examined by scanning electron microscopy (SEM) using Hitachi model S2500. The average grain size, G_{ave} is obtained by multiplying the average linear intercept lengths of the grains by 1.56 [18]. The standard deviation of grain size, ΔG, can be calculated from the statistical equation

$$(\Delta G)^2 = \sum_{i=1}^{n} \frac{(G_i - G_{ave})^2}{n} \quad (3)$$

The grain size range can also be calculated; it is the difference between the largest and smallest values.

After calcination and sintering, crystalline phases of the ceramic samples were identified by powder X-ray diffractometry (Siemens model D5000) using CuK_{α} radiation.

3. Results and discussion

3.1. Sample characteristics

Fig. 1 shows the applied electric field (E) versus current density (J) characteristics of ZnO–glass samples calcined at 600–900 °C for 2 h and 10 h then sintered at 1250 °C for 1 h. Table I gives the data for each specimen: calcination temperature, soaking time at various calcination temperatures, non-linear coefficient (α), V_{br}, non-linear resistance (C) and $\Delta V_{br}/V_{br}$. Specimen S3, calcined at 700 °C, reveals the highest V_{br} among specimens calcined for 2 h at various temperatures then sintered at 1250 °C for 1 h. Whereas specimen S2, calcined at 600 °C for 10 h then sintered at the same condition, possesses the best non-ohmic properties because it reveals the highest α value, largest V_{br} and lowest leakage current ($I_{leak} = 95$ μA) among the ZnO–glass samples studied (Table II).

The process of varistor degradation, as evidenced by increasing I_{leak} and breakdown conduction, can arise from a variety of applied stresses. The estimation of device stability is specified at a condition for which the $\Delta V_{br}/V_{br}$ values of the varistor samples lie within

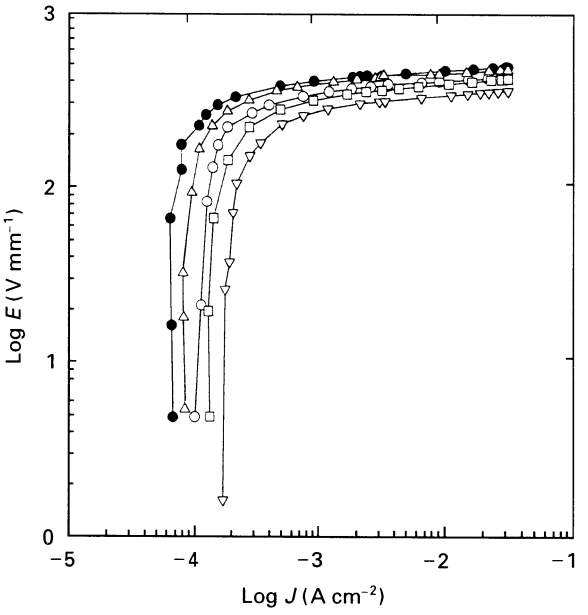

Figure 1 Log–log plot of applied electric field versus current density of the five ZnO–glass specimens (details are given in Table I): (○) S1, (●) S2, (△) S3, (□) S4, (▽) S5.

TABLE I Calcination temperature, soaking time at various calcination temperatures, non-linear coefficient (α), breakdown voltage (V_{br}), non-linear resistance (C), $\Delta V_{br}/V_{br}$, G_{ave}, standard deviation (ΔG), grain size range, minimum grain size (G_{min}) and maximum grain size (G_{max}) of ZnO–glass samples studied

	S1	S2	S3	S4	S5
Calcination temp. (°C)	600	600	700	800	900
Soaking time (h)	2	10	2	2	2
α	24.2	36.63	25.23	18.53	18.98
V_{br}(V)	448	529	474	441	365
C(V mm^{-1})	273	314	304	243	218
$\Delta V_{br}/V_{br}$	>10%	<10%	<10%	<10%	>10%
G_{ave}(μm)	13.98	12.52	13.75	14.52	15.53
ΔG (μm)	2.69	1.06	1.06	1.19	2.70
Range, $G_{max} - G_{min}$ (μm)	10.6	3.55	3.09	4.6	10
G_{min} (μm)	9.4	10.65	12.15	12	10
G_{max} (μm)	20	14.2	15.24	16.6	20

TABLE II Leakage current (I_{leak}), clamping voltage (V_c), peak current (I_{load}) and dynamic resistance ($R_{ZnO-glass}$) of ZnO–glass samples studied

	S1	S2	S3	S4	S5
I_{leak}(μA)	130	95	120	165	212
V_c(V)	700	850	750	650	600
I_{load}(A)	11.50	8.36	10.46	12.54	13.58
$R_{ZnO-glass}$ (Ω)	60.96	101.67	71.70	51.92	44.18

$\pm 10\%$ after a maximum surge current of 26.1 A. Fig. 2 shows variations of V_{br} for all the samples after 60 surge tests. The upper and lower limit lines on each plot represent $V_{br} + 10\%\ V_{br}$ and $V_{br} - 10\%\ V_{br}$, respectively. It may be seen that $\Delta V_{br}/V_{br}$ values of specimens S2, S3 and S4 lie within $\pm 10\%$, even at 26.1 A peak current, but the variations of V_{br} for specimens S1 and S5 reveal poorer device performance after suffering a surge pulse. Therefore, specimens S2, S3 and S4 show better device stability among the samples examined because all ΔV_{br} values of S1 and S5 exceed $\pm 10\%\ V_{br}$ after 10 surge tests, and obvious degradation phenomena are revealed by increasing I_{leak} and decreasing V_{br}. Several authors have observed the degradation phenomena in degraded varistors [19–21]. Gupta and Carlson [20] have reported a grain boundary defect model which assumes that instability in the ZnO varistor arises from field-assisted diffusion of zinc interstitials in the depletion region, followed by chemical interactions with the grain boundary defects. Samples S1 and S5 reveal obvious degradation phenomena, and the electrical properties of ceramic varistors show poorer device stability, although their α values are high enough for commercial applications. Among the samples calcined at various temperatures for different soaking times, specimen S2, calcined at 600 °C for 10 h, possesses the best non-ohmic properties, characterized by the highest α, V_{br} and device stability.

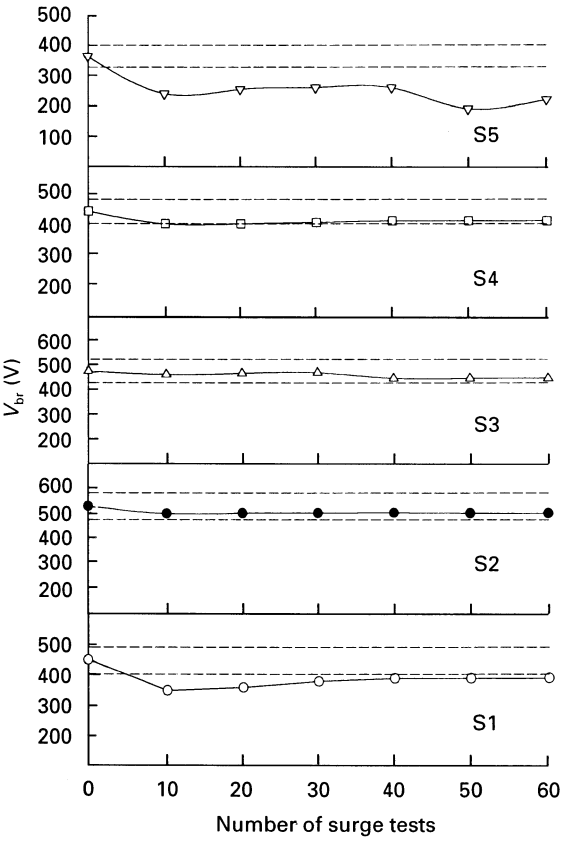

Figure 2 Variations of the breakdown voltage after a total of 60 surge tests for the five specimens investigated.

3.2. Effects of spinel phase formation

It has been reported that ZnO–glass varistors are composed of three phases; ZnO grains, $Zn_7Sb_2O_{12}$ spinel phase and the intergranular layer phase; it has also been reported that the non-ohmic characteristics are enhanced if the intergranular layer phase increases in resistance after it has recrystallized [12, 13]. Fig. 3 shows the XRD patterns of the samples after calcination at various temperatures and for various soaking times. X-ray peak intensities for the XRD patterns were normalized with respect to the intensity of (O, 100) ZnO peaks. The numbers in parentheses in Fig. 3 are the relative intensities of $Zn_7Sb_2O_{12}$ spinel phase; they are the quantitative summation of that phase for each plane. With increasing calcination temperature and calcination time, relative total intensities of the primary spinel phase gradually increase in the calcination process. These results are similar to those obtained for the ZnO–Bi_2O_3 system, as reported by Inada [5]. The relative total intensities of the spinel phase of specimen S2, calcined at 600 °C for 10 h, are much greater than those of specimen S1, calcined for 2 h at the same heat treatment temperature. Therefore, the spinel phase particle can still be formed in ceramic powder after a long soaking time, although the calcination temperature at 600 °C is below the melting point (m.p.) of Sb_2O_3, 656 °C. Specimens S3, S4 and S5, calcined for 2 h at 700, 800 and 900 °C respectively, reveal large amounts of primary spinel phase; this is because their processing temperatures are higher than

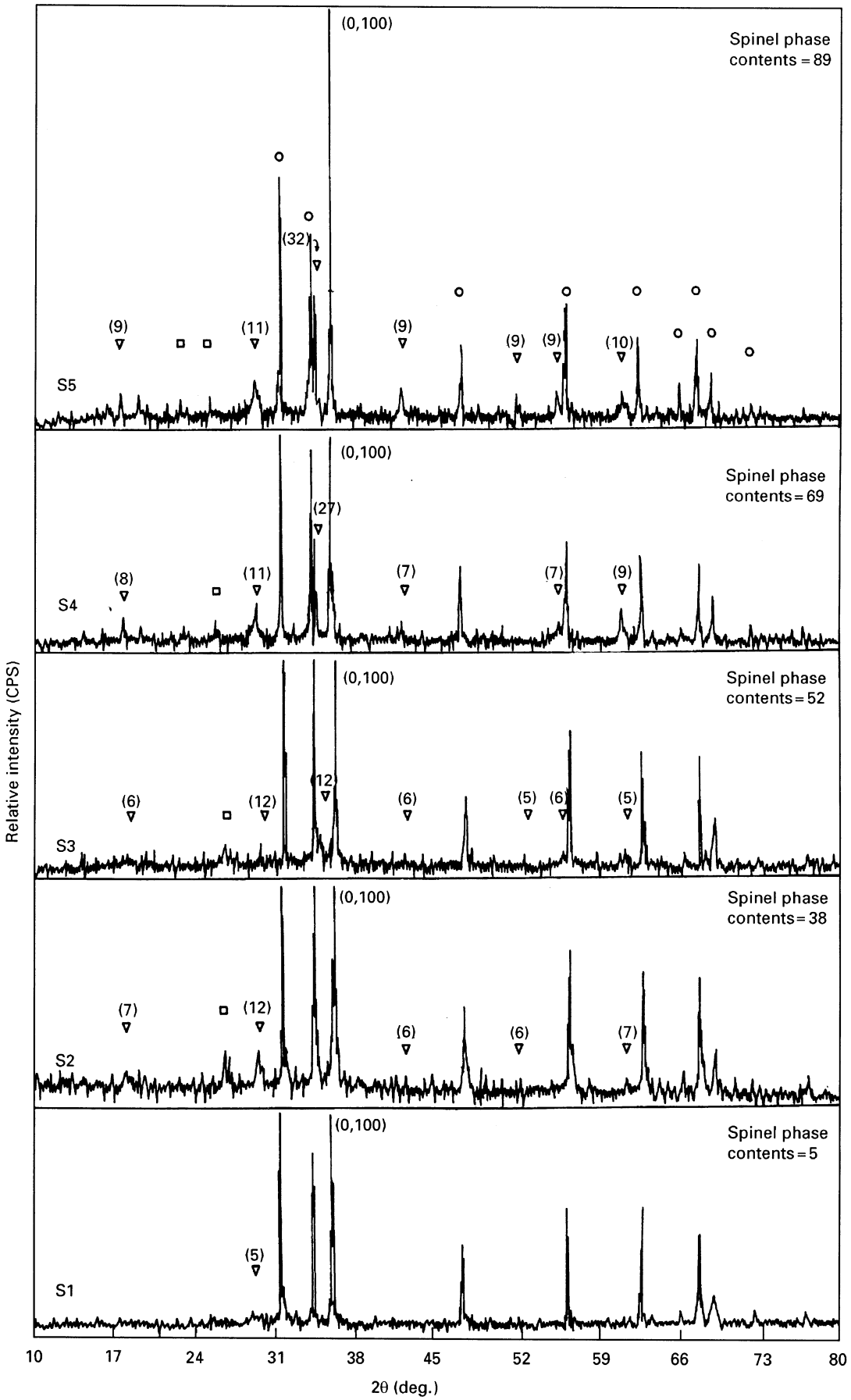

Figure 3 Powder XRD patterns of the five specimens (calcination details in Table I). The diffraction peaks of the three phases are as follows: (○) ZnO, (▽) $Zn_7Sb_2O_{12}$, (□) $2ZnO{\cdot}SiO_2$; the (O, 100) is the normalized (1 0 1) ZnO peak.

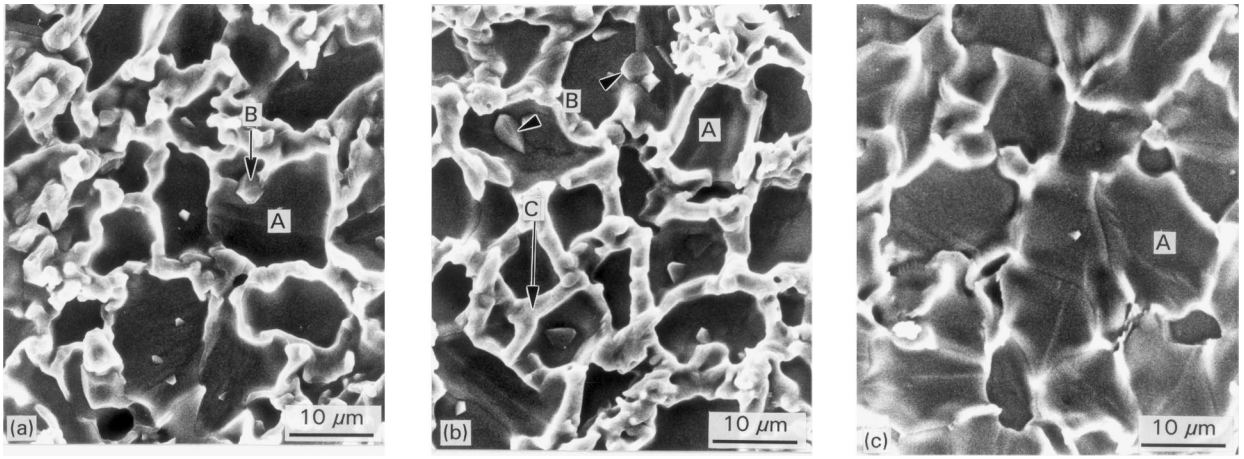

Figure 4 Typical SEM micrographs of (a) specimen S1, (b) specimen S2 and (c) specimen S5. Key to phases: (A) ZnO grain, (B) spinel phase and (C) intergranular glass phase.

the m.p. of Sb_2O_3. The liquid Sb_2O_3 enhances the formation rate of the $Zn_7Sb_2O_{12}$ spinel phase during calcination.

Fig. 4a, b and c show, respectively, the typical SEM micrographs of specimens S1, S2 and S5 sintered at 1250 °C for 1 h. The microstructure of the ZnO–glass samples consists of three phases: (A) ZnO grains; (B) well-faceted spinel grains a few micrometers wide at the boundaries between the ZnO grains (A); and (C) an intergranular glass phase of 1–2 μm forming a vein-like network structure. The statistical distribution of the grain size from SEM examination, including the average grain size (G_{ave}), the standard deviation (ΔG), the grain size range, the minimum grain size (G_{min}) and the maximum grain size (G_{max}) are summarized in Table I. It indicates that specimen S2, calcined at 600 °C for 10 h, possesses the smallest average grain size ($G_{ave} = 12.52$ μm) among the investigated samples and reveals narrower grain size range (10.65 ~ 14.2 μm) and uniform size distribution; whereas specimen S1, calcined at the same temperature for 2 h, possesses larger G_{ave} (13.98 μm) and shows non-uniform size distribution associated with wider grain size range (9.4 ~ 20 μm), from the SEM micrographs. On the other hand, specimen S5, calcined at 900 °C for 2 h, has the largest G_{ave} (15.53 μm) and also shows a non-uniform grain size distribution associated with a wider range of grain size (10 ~ 20 μm).

Fig. 5 shows the XRD patterns of the investigated specimens after sintering at 1250 °C for 1 h. It also shows the relative intensities of the spinel phase for each plane with respect to (O, 100) ZnO peak. The relative total intensities of specimens S1 and S2 after being sintered (contents of spinel phase = 149) are obviously larger than those of specimens S3 (104), S4 (102) and S5 (90), all heat treated at the same sintering condition. As shown in Fig. 3, a much smaller amount of primary spinel phase for specimen S1 was included in calcined powder after being calcined for 2 h at 600 °C, below the m.p. of Sb_2O_3; therefore, a large amount of spinel phase is formed in specimen S1 after sintering. It is expected that the spinel particles non-uniformly distribute in the varistor microstructure, thus the effect of inhibiting ZnO grain growth is limited during the sintering process; finally, ZnO grains have grown non-uniformly, as sown in Fig. 4a, i.e. unstable ZnO varistors are formed. Bowen and Avella [22] have reported a large spread in grain size for ZnO sintered with Al_2O_3 additive; they ascribed this to discontinuous grain growth. Moreover, high local currents and overload are caused by a few large single grains, which give rise to rapid degradation of the varistor in electrical pulse operation. Hence, careful control of the microstructure of the ZnO material is needed to obtain good device stability.

Hennings *et al.* [11] have used seed grains in ZnO varistors to produce uniform grain growth, and their varistors revealed the narrow distribution of the electrical values around a mean value. Therefore, specimen S1, calcined at 600 °C for 2 h, possesses lower V_{br} and poorer device stability than specimen S2 because it has non-uniform grain size distribution S1 (9.4 ~ 20 μm), as shown in Table I. The optimum amount of primary spinel phase (38) was formed in specimen S2 during calcination at 600 °C for 10 h; this shows that the phase grows and distributes uniformly in the subsequent sintering process and effectively inhibits ZnO grain growth (Fig. 4b). Specimen S2 reveals the largest V_{br} and the smallest G_{ave} and possesses good device stability as a result of its smaller grain size range (Table I). And, as shown in Fig. 5, a larger amount of crystalline intergranular layer phase exists in specimen S2 than in the other specimens; it possesses the best non-ohmic properties, characterized by the highest α value. This result coincides with the previous reports [12, 13]. Therefore, specimen S2 possesses the best non-ohmic properties, characterized by the highest α, V_{br} and device stability.

As shown in Fig. 3, spinel phase was also included in specimens S3 and S4, during the calcination process, and it is expected that the spinel phase grows and distributes uniformly. Therefore, specimens S3 and S4 possess uniform grain size distribution, by effectively inhibiting ZnO grain growth during the sintering process, and they have good device stability. On the other hand, specimen S5, calcined at a higher temperature than the m.p. of Sb_2O_3, shows the lowest V_{br} and the largest G_{ave}; its poorer device stability results from

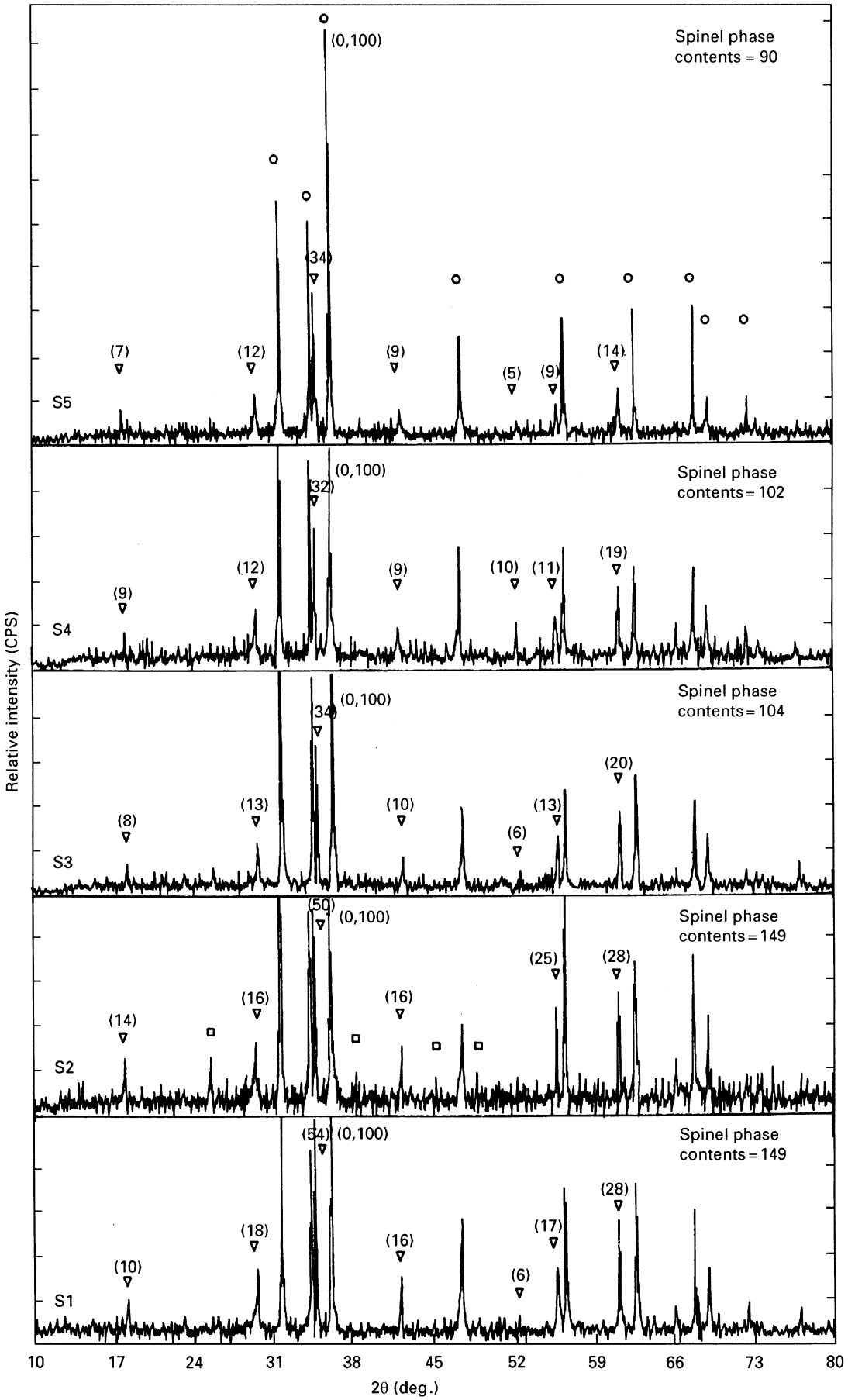

Figure 5 Powder XRD patterns of the five specimens after sintering. See Fig. 3 for key to symbols.

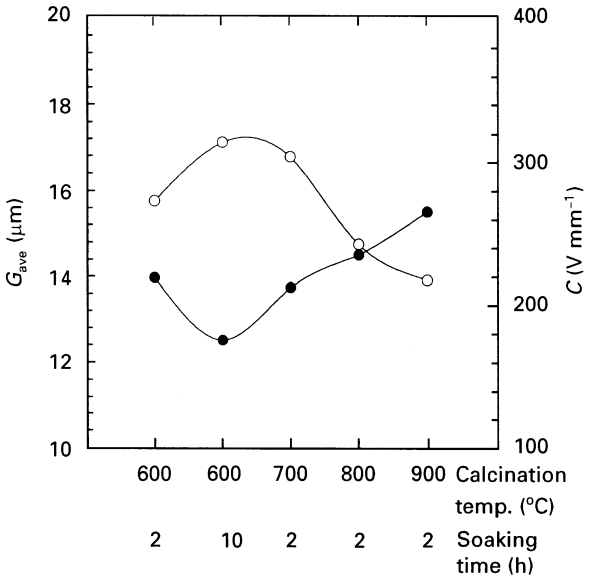

Figure 6 Relationship between (●) the average grain size, G_{ave}, and (○) the non-linear resistance, C, for the five specimens investigated.

a non-uniform grain size distribution (10 ~ 20 μm). It could be considered from the XRD pattern of specimen S5 that, after being sintered, there is a decrease in the net amount of spinel phase – caused by vaporization of part of the Sb_2O_3 at 900 °C – so there remains in the varistor a relatively small amount of spinel phase to inhibit ZnO grain growth. The optimum amount of primary spinel phase, formed during the calcination process, that can inhibit ZnO grain growth in the subsequent sintering process plays a prominent role in determining the grain size distribution, V_{br} and device stability of ZnO–glass ceramic varistors. Uniform grain size distribution obtained from a suitable calcination process is an important microstructural parameter in achieving good device stability of ZnO–glass varistors on the basis of the results of stability tests and the statistical distribution of grain size indicated in Table I.

The voltage at the onset of non-linearity is the non-linear voltage. However, from Equation 1, this non-linear voltage can be defined as

$$C = \frac{V}{I^{1/\alpha}} = V \quad \text{at 1 mA} \tag{4}$$

Using this definition, V_{br} in the literature has often been described as the voltage observed at 1 mA ($V_{1\ mA}$). This also implies that the non-linear voltage, C, is a resistance unit ($V_{1\ mA}$/1 mA). The non-linear resistance, C, is defined by a voltage drop per unit length (V mm^{-1}) when 1 mA cm^{-2} of current flows through the body. By using this definition, the non-linear resistance can be read from the E–J curves of Fig. 1. Fig. 6 shows the relationship between G_{ave} and C for the samples using different calcination processes. It indicates that the non-linear resistance of the examined samples increases as the average grain size decreases. The data are displayed as a function of calcination temperature. This phenomenon is in good agreement with the result reported by Mah *et al.* [8]. Another parameter correlated with average grain size will be introduced in the next section.

3.3. Pulse response and dynamic resistance

The typical surge responses, which display schematic voltage (V) and current (I) waveforms respectively using scale factors 1/200 and 1/100, for specimens S2 and S5 are shown in Fig. 7a and b. The circuit of a constant current source surge generator with applied voltage (V_{ap}) and a schematic microstructure of the ZnO–glass varistors are depicted in Fig. 8. Between two terminals of the investigated bulk varistors, there is a series connection of ZnO grains and the intergranular glass layer along the conduction paths. Consider the circuit of Fig. 8 with V_{ap} driving the examined specimens, which clamp at V_c, and with I_{load} flowing into the varistors. According to the circuit diagram

$$I_{load} = (V_{ap} - V_c)/R \tag{5}$$

$$R_{ZnO\text{–}glass} = V_c/I_{load} \tag{6}$$

where R is the network resistance (48 Ω) of the surge generator, V_c is the clamping voltage across the sample and $R_{ZnO-glass}$ is the dynamic resistance of the bulk varistor. Table II summarizes the measured parameters, derived from the surge response schematics in Fig. 7 and calculated from Equations 5 and 6. I_{leak} represents the leakage current of the varistor at room temperature when the voltage value is 0.8 V_{br}. From Table II, specimen S2 reveals the highest clamping voltage (V_c = 850 V), the lowest peak current (I_{load} = 8.36 A) and the largest dynamic resistance

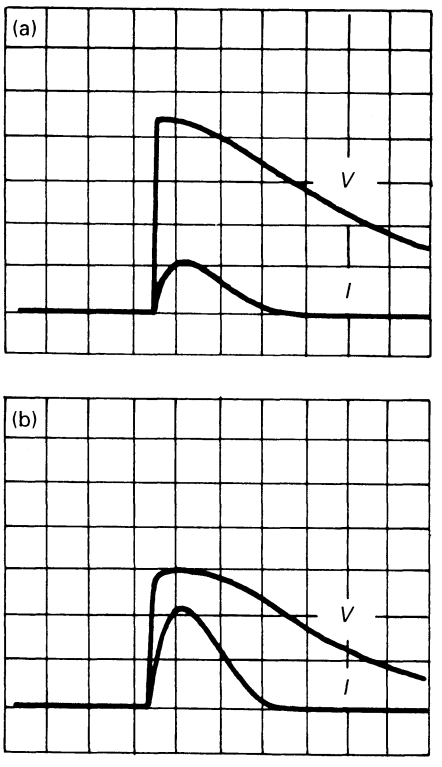

Figure 7 Typical voltage and current surge response waveforms for (a) specimen S2 and (b) specimen S5. Vertical scales: V, 200 V per division; I, 5 A per division. Horizontal scale: t, 10 μs per division.

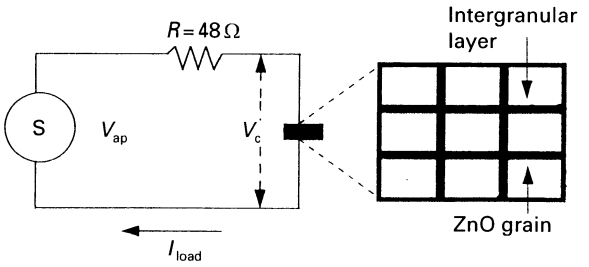

Figure 8 Circuit for the constant current source surge generator with applied voltage (V_{ap}) and schematic microstructure of the ZnO–glass varistors.

($R_{ZnO-glass} = 101.67\ \Omega$) among the examined specimens of constant thickness; this is because it possesses the lowest G_{ave} and the highest V_{br}. In contrast, specimen S5, with the highest G_{ave} and lowest V_{br}, has the smallest V_c, the smallest $R_{ZnO-glass}$ and the largest I_{load} on the basis of Fig. 7b. The clamping voltage and the dynamic resistance of the samples increased as the average grain size decreased (Table II). It is suggested that the smaller average grain size contributes to the larger series resistance of the ZnO–glass samples at the same thickness; meanwhile, the larger series resistance resulted in a lower peak current during surge impact. Moreover, the tendency of the dynamic resistance ($R_{ZnO-glass}$) of the investigated samples is in accordance with that of the non-linear resistance (C) with the variation of the average grain size, as shown in Fig. 6. These two parameters, associated with the average grain size, apparently imply the insulating characteristics of the varistor sample in the non-linear breakdown region.

Variations of the leakage current and the dynamic resistance for the examined samples are shown in Fig. 9. It reveals opposite tendencies between I_{leak} and $R_{ZnO-glass}$ with the different calcination processes. The leakage current of the samples decreases with an increase in the dynamic resistance because the average grain size is decreased. According to the schematic microstructure in Fig. 8, the dynamic resistance of the ZnO–glass samples during surge impact consists of two parameters: the resistance of the ZnO, R_{ZnO} and the resistance of the intergranular glass layer, R_{glass}, proportional to the number of intergranular layers per unit length. It is well known that R_{ZnO} is nearly constant at the same thickness for each specimen, but R_{glass} is much greater than R_{ZnO} per unit length [13]. Therefore, the dynamic resistance obtained from the combined voltage–current surge waveforms is determined by the resistance of the intergranular layer per unit length, i.e. the number of intergranular layers at the same thickness. Specimen S2, with the smallest G_{ave}, possesses the greatest number of intergranular layers among the investigated samples of constant thickness, therefore, the largest dynamic resistance and non-linear resistance can be obtained in specimen S2. The converse applies to specimen S5, with the largest G_{ave}. Increases of the dynamic resistance and non-linear resistance, caused by decreasing the grain size, would ultimately enhance the sample clamping voltage and sample breakdown voltage, respectively.

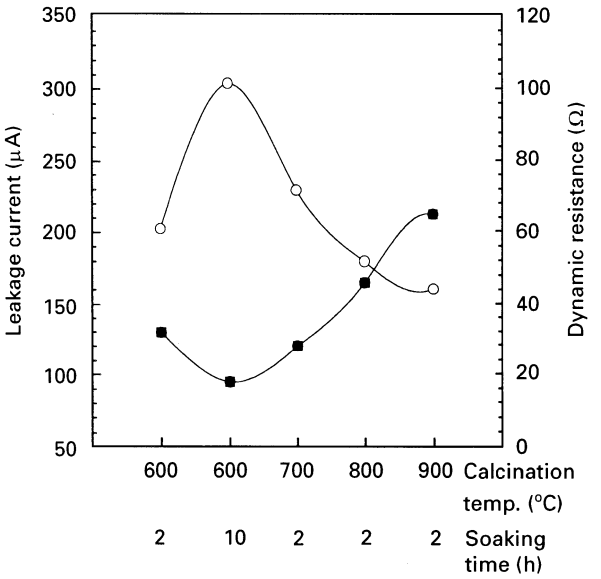

Figure 9 Variations of (■) leakage current and (○) dynamic resistance for the five specimens investigated.

This would be accompanied by a lower leakage current because there would be an increase in the number of intergranular layers per unit length. The dynamic resistance, correlated with the non-linear resistance of the ZnO–glass varistor, was proposed to describe the insulating characteristics of the varistor samples.

4. Conclusions

This study investigated the influence of various calcination processes on the formation of spinel phase during sintering, including the effects of different temperatures and soaking times. The $Zn_7Sb_2O_{12}$ spinel phase was formed during calcination and could inhibit ZnO grain growth during sintering; it plays an important role in determining the grain size distribution and the device stability of ZnO–glass ceramic varistors. A wide range in grain size, due to discontinuous ZnO grain growth, was possibly caused by a non-uniform distribution of spinel particles when they were formed at calcination, or by vaporization of a part of the Sb_2O_3 at a higher calcination temperature. The samples having non-uniform grain size gave rise to rapid degradation in electrical pulse operation. Whereas the sintered samples obtained from suitably calcined powders revealed the narrow distribution of grain size and good device stability.

The dynamic resistance ($R_{ZnO-glass}$) obtained from the voltage–current surge waveforms and the non-linear resistance would be good parameters to evaluate the insulating characteristics of ZnO–glass varistor samples. In the investigated samples, dynamic resistance and non-linear resistance per unit length increased with decreasing average grain size. It appears that these two characteristic parameters respectively caused the increases in sample clamping voltage and sample breakdown voltage. And the intergranular layer phase that existed in the grain boundaries of the specimen S2 enhanced its non-ohmic properties by

raising the non-linear coefficient and lowering the leakage current.

Acknowledgement

We gratefully acknowledge support from the National Science Council of China under project NSC 83-0404-009-088.

References

1. M. MATSUOKA, *Jpn J. Appl. Phys.* **10** (1971) 736.
2. J. WONG and W. G. MORRIS, *Amer. Ceram. Soc. Bull.* **53** (1974) 816.
3. J. WONG, *J. Appl. Phys.* **51** (1980) 4453.
4. T. K. GUPTA, *J. Amer. Ceram. Soc.* **73** (1990) 1817.
5. M. INADA, *Jpn J. Appl. Phys.* **17** (1978) 1.
6. *Idem*, *ibid.* **19** (1980) 409.
7. J. WONG, *J. Appl. Phys.* **46** (1975) 1653.
8. J. P. MAH, J. S. CHOI and S. H. PEAK, *J. Mater. Sci.* **25** (1990) 3375.
9. P. R. EMTAGE, *J. Appl. Phys.* **50** (1979) 6833.
10. S. N. BAI, J. S. SHIEH and T. Y. TSENG, *Mater. Chem. Phys.* **41** (1995) 104.
11. D. F. K. HENNINGS, R. HARTUNG and P. J. L. REIJNEN, *J. Amer. Ceram. Soc.* **73** (1990) 645.
12. Y. S. LEE and T. Y. TSENG, *ibid.* **75** (1992) 1636.
13. Y. S. LEE and T. Y. TSENG, *J. Mater. Sci. Mater. Elec.* (submitted).
14. T. TAKEMURA, M. KOBAYASHI, Y. TAKADA and K. SATO, *J. Am. Ceram. Soc.* **70** (1987) 237.
15. A. T. SANTHANAM, T. K. GUPTA and W. G. CARLSON, *J. Appl. Phys.* **50** (1979) 852.
16. J. C. KIM and E. GOO, *J. Mater. Sci.* **24** (1989) 76.
17. T. ASOKAN and R. FREER, *ibid.* **25** (1990) 2447.
18. M. I. MENDELSON, *J. Amer. Ceram. Soc.* **52** (1969) 443.
19. K. EDA, A. IGA and M. MATSUOKA, *J. Appl. Phys.* **51** (1980) 2678.
20. T. K. GUPTA and W. G. CARLSON, *J. Mater. Sci.* **20** (1985) 3487.
21. S. N. BAI and T. Y. TSENG, *J. Amer. Ceram. Soc.* **78** (1995) 2685.
22. L. J. BOWEN and F. J. AVELLA, *J Appl. Phys.* **54** (1983) 2764.

Received 4 April
and accepted 8 October 1995